Title

Reevaluating the imaging definition of tumor progression: perfusion MRI quantifies recurrent glioblastoma tumor fraction, pseudoprogression, and radiation necrosis to predict survival

Authors

Hu, Leland S
Eschbacher, Jennifer M
Heiserman, Joseph E
et al.

NEURO-ONCOLOGY

Reevaluating the imaging definition of tumor progression: perfusion MRI quantifies recurrent glioblastoma tumor fraction, pseudoprogression, and radiation necrosis to predict survival

Leland S. Hu*, Jennifer M. Eschbacher, Joseph E. Heiserman, Amylou C. Dueck, William R. Shapiro, Seban Liu, John P. Karis, Kris A. Smith, Stephen W. Coons, Peter Nakaji, Robert F. Spetzler, Burt G. Feuerstein, Josef Debbins, and Leslie C. Baxter

Department of Radiology (L.S.H.); Department of Biostatistics (A.C.D.), Mayo Clinic in Arizona, Phoenix, Arizona; Department of Neuropathology (J.M.E.); Keller Center for Imaging Innovation (L.S.H., S.L., J.P.K., J.D., L.C.B.); Department of Neuroradiology (J.E.H., J.P.K.); Department of Neurosurgery (K.A.S., P.N., R.F.S.); Department of Neurology (W.R.S., B.G.F.) at the Barrow Neurological Institute-St. Joseph's Hospital and Medical Center, Phoenix, Arizona; University of Arizona College of Medicine, Phoenix, Arizona (B.G.F.)

INTRODUCTION: Contrast-enhanced MRI (CE-MRI) represents the current mainstay for monitoring treatment response in glioblastoma multiforme (GBM), based on the premise that enlarging lesions reflect increasing tumor burden, treatment failure, and poor prognosis. Unfortunately, irradiating such tumors can induce changes in CE-MRI that mimic tumor recurrence, so called post treatment radiation effect (PTRE), and in fact, both PTRE and tumor re-growth can occur together. Because PTRE represents treatment success, the relative histologic fraction of tumor growth versus PTRE affects survival. Studies suggest that Perfusion MRI (pMRI)–based measures of relative cerebral blood volume (rCBV) can noninvasively estimate histologic tumor fraction to predict clinical outcome. There are several proposed pMRI-based analytic methods, although none have been correlated with overall survival (OS). This study compares how well histologic tumor fraction and OS correlate with several pMRI-based metrics. **METHODS:** We recruited previously treated patients with GBM undergoing surgical re-resection for suspected tumor recurrence and calculated preoperative pMRI-based metrics within CE-MRI enhancing lesions: rCBV mean, mode, maximum, width, and a new thresholding metric called pMRI–fractional tumor burden (pMRI-FTB). We correlated all pMRI-based metrics with histologic tumor fraction and OS. **RESULTS:** Among 25 recurrent patients with GBM, histologic tumor fraction correlated most strongly with pMRI-FTB ($r = 0.82$; $P < .0001$), which was the only imaging metric that correlated with OS ($P<.02$). **CONCLUSION:** The pMRI-FTB metric reliably estimates histologic tumor fraction (i.e., tumor burden) and correlates with OS in the context of recurrent GBM. This technique may offer a promising biomarker of tumor progression and clinical outcome for future clinical trials.

Keywords: glioblastoma, histologic tumor fraction, perfusion MRI, pseudoprogression, radiation necrosis, recurrent, relative cerebral blood volume, survival.

As drug discovery programs search for new treatment strategies to improve the survival of patients with glioblastoma multiforme (GBM), the need for a timely and accurate end point to judge treatment

efficacy has never been greater.[1] Overall survival (OS) represents the benchmark measure of outcome but has clear disadvantages for clinical trial assessment. Clinical trials that use OS are lengthened because of the time needed to observe mortality,[1,2] and correlations between OS and initial treatment are modified by subsequent salvage therapies.[2,3] These limitations have led to the use of progression-free survival (PFS) as a surrogate marker for OS. However, PFS requires accurate estimates of tumor growth based on MRI, and such estimates are not always readily made, nor does PFS correlate well with OS.[2,3]

Contrast-enhanced MRI (CE-MRI) represents the best available method for measuring treatment response and predicting survival after standard first-line therapy and is used to define PFS.[2-4] Currently, decisions about treatment are guided by criteria (Macdonald, RANO) that equate increasing size of CE-MRI enhancement with progressive tumor burden, treatment failure, and poor prognosis.[5,6] Despite its widespread use, this approach has distinct limitations. First, CE-MRI cannot distinguish tumor growth from treatment-induced parenchymal injury, so called post-treatment radiation effect (PTRE), which exactly mimics tumor on CE-MRI. Two well documented forms of PTRE are pseudoprogression (pP) and radiation necrosis (RN). Unlike tumor, PTRE represents a positive response to treatment and, therefore, a good prognosis; however, PTRE-related enhancement underlies erroneous declaration of treatment failure in up to half of cases.[7-10]

In addition, tumor often coexists and variably admixes with PTRE in most patients.[11] The histologic tumor fraction (i.e., tumor burden) therefore comprises a subcomponent of the total CE-MRI enhancement and represents a potentially useful predictor of survival in patients with recurrent brain tumor.[12-14] In fact, studies suggest that histologically quantifying tumor burden provides more meaningful prognostic information than simply reporting the presence of tumor.[12-15] Because CE-MRI cannot reliably distinguish the coexistence of PTRE and tumor burden, surgical biopsy and histologic evaluation remain the current benchmark.[13] Unfortunately, surgery is not without medical risk, morbidity, and cost. These issues underscore a clear need to develop a noninvasive method to accurately estimate tumor burden as a potential alternative or adjunct to surgical biopsy.

Perfusion MRI (pMRI) noninvasively detects GBM and PTRE microvascular characteristics, most commonly with the dynamic susceptibility-weighted contrast-enhanced (DSC) method. With use of pMRI, relative cerebral blood volume (rCBV) is measured on a voxel-wise basis across CE-MRI lesions, providing regionally specific estimates of tissue microvasculature and histologic identity.[16-24] To date, several pMRI-based analytic methods have been proposed to estimate histologic tumor fraction, each with potential advantages and limitations. First, calculating mean rCBV across all CE-MRI lesion voxels is the easiest method but does not assess intervoxel variations that may reflect histologic heterogeneity.[16,17] Second, histogram analysis contributes additional metrics, including mode, maximum, and histogram width, although these may be biased by spatial statistics.[18,19] Finally, the voxel-

based thresholding method applies predetermined rCBV criteria to classify individual voxels based on histologic identity, but requires that the accuracy of the threshold be prospectively validated.[20,21]

To date, no published studies support consensus regarding which pMRI-based analytic method best estimates histologic tumor fraction as a predictor of survival in recurrent GBM. Our hypothesis is that tumor burden and OS will correlate more strongly with those pMRI-based methods that use a voxel-based approach to assess histologic heterogeneity. We here report a study in a cohort of patients with recurrent GBM with CE-MRI evidence of tumor progression. Our goals were to (1) determine the strengths of correlation between histologic tumor fraction and previously published pMRI-based metrics (rCBV mean, mode, maximum, and histogram width) and a new voxel-based thresholding metric, called pMRI fractional tumor burden (pMRI-FTB), and (2) identify which pMRI-based metric best correlates with OS.

Methods

Patients

We recruited patients with recurrent GBM undergoing image-guided stereotactic surgical re-resection of newly developed or enlarging lesions identified on surveillance CE-MRI. Prior to enrollment, all study patients had undergone surgery and received temozolomide (TMZ) and radiation therapy (RT) according to the Stupp protocol.[4] We documented the timing of CE-MRI lesion development relative to prior treatment, excluded subjects with estimated glomerular filtration rate (eGFR) <60 mg/min/1.72m^2, and obtained approval from the Institutional Review Board and written informed consent from each subject. The histopathology and MRI data were obtained and recorded independently of each other before correlation was determined.

Preoperative DSC-MRI Protocol

We used a 3 Tesla MR system (General Electric Medical Systems) for all patients. After antecubital fossa or forearm intravenous catheter placement and 6 minutes prior to the DSC-MRI acquisition, we administered 0.1 mmol/kg Gd-DTPA contrast agent (gadodiamide or gadobenate dimeglumine) preload dose to minimize T1W leakage effects.[22-25] During acquisition, we gave 0.05 mmol/kg bolus at 3–5 cc/sec.[22-25] The DSC-MRI sequence parameters were: Gradient-echo Echo Planar Imaging (EPI) with TR (msec)/TE (msec)/ flip angle $= 1500-2000/20/60°$; FOV 24×24 cm, matrix 128×128, 5 mm slice; no interslice gap. These parameters yielded an in-plane spatial resolution of 1.8×1.8 mm and voxel volumes of 0.02 cm^3. The total Gd-DTPA dose was 0.15 mmol/kg body weight.

Preoperative Stereotactic Anatomical Data Set

We obtained pre- and postcontrast T1W Spoiled Gradient-Echo (SPGR-IR prepped) stereotactic MRI data sets (TI/TR/TE = 300/6.8/2.8 msec; matrix 320 × 224; FOV = 26 cm; slice thickness = 2 mm) before and after DSC-MRI for neuronavigation during surgical resection. We performed all imaging within one day of surgery. We used IB Suite (v. 1.0.454) (Imaging Biometrics) to coregister the stereotactic anatomical images with the DSC-MRI data and rCBV maps, using multiple registration methods implemented in ITK, the Insight Segmentation and Registration Toolkit (www.itk.org), similar to previously described methods.[19,20,22,23]

Relative Cerebral Blood Volume (rCBV) and rCBV Map Generation

We used an Osirix (v. 3.6.1) workstation with IB Neuro (v. 1.1.430) and IB Suite (v. 1.0.454) (Imaging Biometrics) software to calculate whole-brain rCBV maps from the DSC data, coregistered to stereotactic data. RCBV was calculated based on well-established methods.[22–24] In short, after excluding the first 4 time points of each DSC-MRI series due to saturation effects, we normalized signal intensity (SI) to baseline and converted series to change in relaxivity over time $[\Delta R2^*(t)]$ for the entire brain. We generated CBV maps by integrating the area under the $\Delta R2^*(t)$ curve, ending at the time point forty seconds after the nadir SI of the first pass-bolus. All CBV values were corrected for T1W leakage with preload dosing, and a modeling algorithm was used to correct T2/T2*W residual effects.[23] CBV maps were normalized to contralateral normal appearing white matter (NAWM) to create rCBV maps.[22–24]

Acquisition of Surgical Tissue, Criteria for Histologic Diagnosis, and Estimation of Histologic Tumor Fraction

For all patients, we collected surgical tissue intraoperatively from multiple stereotactic biopsies and surgical resection, and we used only tissue collected from contrast-enhancing portions of the CE-MRI lesions for the purposes of this study. We fixed all surgical tissue specimens in 10% formalin, embedded in paraffin, sectioned (10-micron), and H&E stained per standard diagnostic protocol at our institution. Two neuropathologists recorded the presence and quantity of GBM and/or PTRE elements for all specimens without knowledge of DSC-MRI results.[11,12,26] In short, for all submitted surgical tissue, 2 neuropathologists simultaneously estimated the histological fractional volume of tumor relative to nonneoplastic features, based on relative fractions of treatment effects versus neoplastic features, as previously described.[12–15,18,20] Both neuropathologists reached a concordance on the majority of cases reviewed. The rare case for which there was disagreement was re-reviewed and a concordant diagnosis was

reached. Some cases had multiple slides available for review. These cases were noted to be difficult to evaluate because of the numbers of slides. Areas of tumor and PTRE were marked on each slide, grossly measured, microscopically re-evaluated, and a concordance reached on percentage of tumor/PTRE.

PTRE features included pauci-cellularity, scattered rare or no atypical cells, lack of mitotic figures except in inflammatory cells, preponderance of reactive cells including astrocytes (gemistocytes), microglia and macrophages, and vascular hyaline fibrosis. Necrosis, often circumscribed in nonneoplastic parenchyma, if present, was considered to be specific for PTRE. Features of tumor recurrence included cellular sheets and/or nests of atypical cells often with mitotic figures. If necrosis was present, it was a minor component of the cellular tumor rather than parenchyma. The finding of fewer atypical cells, in a linear infiltrative configuration in parenchyma without prominent reactive changes, was also classified as recurrence.

Classifying Stereotactic Tissue Specimens and Determining an Optimal rCBV Threshold to Distinguish GBM and PTRE

In an initial subset of 26 stereotactic biopsy samples from the first 9 patients with GBM in our series, we recorded the biopsy locations during neuronavigational surgery[21] and categorized all biopsy specimens as either tumor or PTRE on the basis of the aforementioned histologic criteria. Consistent with prior convention, samples containing a mixture of both GBM and PTRE were classified as tumor, regardless of the degree of admixture.[12,21,27] Only samples with pure radiation change (in the absence of tumor criteria) were categorized as PTRE. The presence of a few isolated, scattered atypical cells did not qualify as tumor categorization if other neoplastic features were absent. For each biopsy sample, we placed a coregistered 3 × 3 voxel (~0.3 cm²) region of interest (ROI) centrally within corresponding recorded stereotactic locations, yielding a localized mean rCBV that was correlated with the categorization of tumor or PTRE. We evaluated each rCBV value as a potential threshold value to distinguish PTRE and tumor across all 26 biopsy samples. At each rCBV cutoff, we determined the sensitivity, specificity, 95% confidence intervals (CI), and accuracy (defined as the average of sensitivity and specificity) for distinguishing PTRE and tumor. We defined the optimal threshold rCBV as the value that yielded the highest accuracy, and we used this threshold for all subsequent analyses to classify individual voxels as tumor or PTRE.

Correlating Intervoxel rCBV Variability and Histologic Heterogeneity for Stereotactic Biopsy Samples Containing Tumor

Previous studies using the binary classification of tissue samples as tumor and PTRE reported broad variability

in the degree of histologic admixture within the tumor category.[13–16,18,20] We used the initial set of 26 biopsy samples (from 9 patients) to test whether the voxel-based application of our optimized threshold could estimate tumor/PTRE admixture within the biopsy samples containing tumor. To accomplish this, we studied the intervoxel rCBV variability within each 3×3 voxel-sized ROI corresponding to the biopsy samples that were categorized as tumor. For each ROI, we calculated

the percentage of voxels with rCBV above threshold (determined in the previous section) that were predictive of tumor. We used Pearson correlation to compare this percentage with the histologic tumor fraction from each biopsy (using the histologic criteria described above) ($P < .05$). Similarly, we correlated the rCBV mean (of all 9 voxels) for each ROI with the histologic tumor fraction from corresponding biopsy samples that were categorized as tumor.
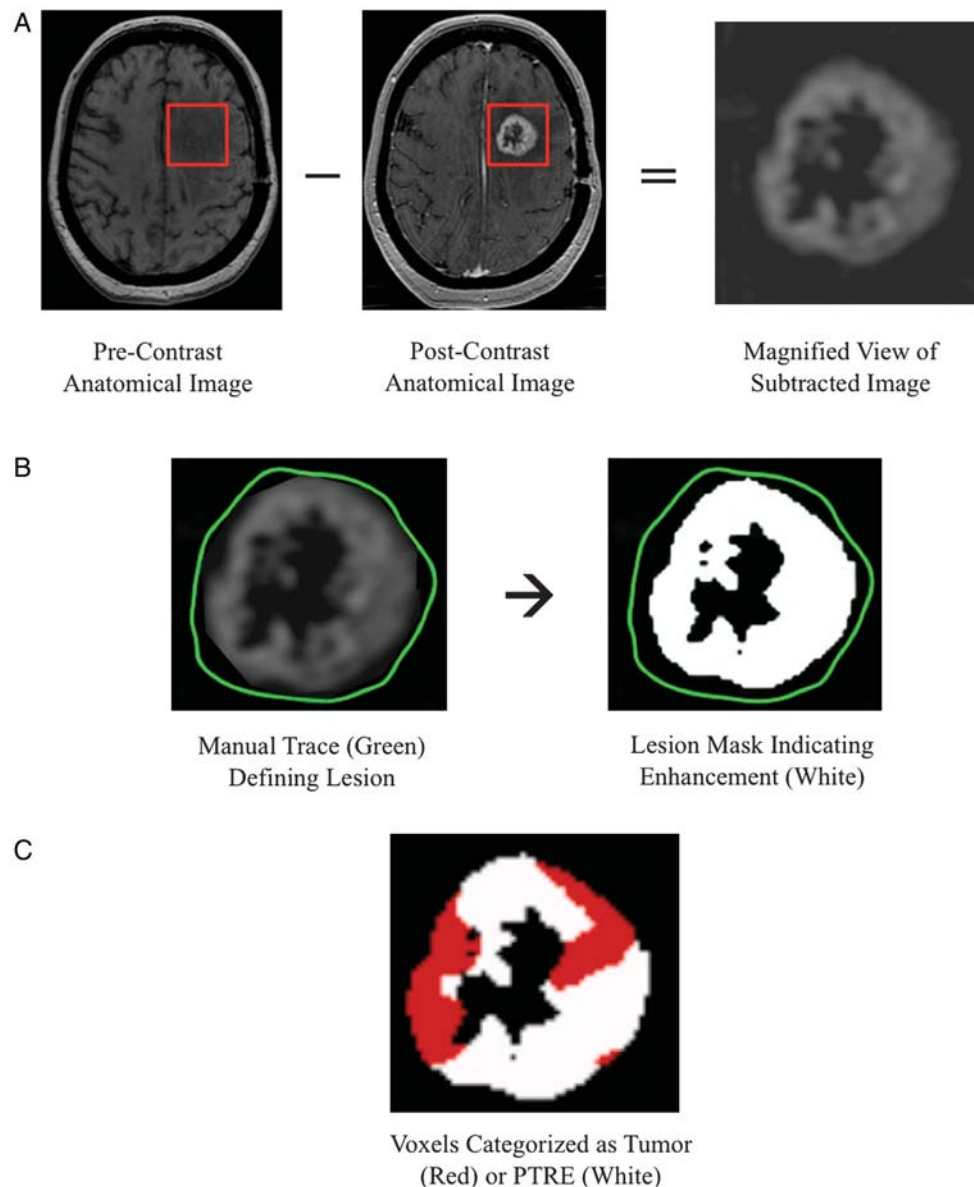

Fig. 1. Flow Diagram for Calculation of Perfusion MRI-Fractional Tumor Burden (pMRI-FTB). The pMRI-FTB metric is calculated for CE-MRI enhancing lesions using the following algorithm: (A) we subtracted pairs of voxel values between coregistered precontrast (left) and postcontrast (middle) anatomical images to identify enhancing tissue (right); (B) we establish a Volume of Interest (VOI) (left, green line) by manually tracing the periphery of enhancing lesions, excluding visible surrounding vascular structures. Based on signal intensity ranges within the VOI (right), a lesion mask is created that includes enhancing voxels (white) and excludes nonenhancing and necrotic voxels (black); 3) Following coregistration with the rCBV map, the lesion mask voxels are categorized as tumor (red) or PTRE (white) based on the optimized rCBV threshold (shown in Fig. 1C). We defined pMRI-FTB as the percentage of tumor voxels relative to total lesion mask voxels.

pMRI-FTB

For all patients in this study (including the initial set of 9 patients), we calculated pMRI-FTB within entire CE-MRI enhancing lesions using the following algorithm (summarized in Fig. 1): we subtracted pairs of voxel values between coregistered pre- and postcontrast anatomical images to identify enhancing tissue; we established a volume of interest (VOI) by manually tracing the periphery of enhancing lesions, excluding visible surrounding vascular structures. Based on signal intensity ranges within the VOI, a lesion mask was created to include enhancing voxels and exclude nonenhancing and necrotic voxels. After coregistration with rCBV maps, the lesion mask voxels were categorized as tumor or PTRE based on the optimized rCBV threshold (determined in the section above). We defined pMRI-FTB as the percentage of tumor voxels relative to total lesion mask voxels.[20] We excluded any visible regions of decreased signal on EPI native images prior to contrast bolus arrival suggestive of blood products or susceptibility artifact typically observed at the skull base due to air-brain interfaces.[21]

Mean rCBV and Other rCBV Histogram Metrics

For all patients in this study (including the initial set of 9 patients), we analyzed all voxels within enhancing lesion masks as defined in the pMRI-FTB section above to calculate other rCBV metrics based on histogram analysis.[16,18,19] We calculated mean rCBV as the average of all rCBV values from the lesion mask voxels[16,17] and generated histograms based on previously published methods.[18,19] In short, histograms were first generated by classifying all lesion mask rCBV values into a predefined number of bins. We divided the interval between the minimum and maximum voxel values into 108 equally spaced bins, counted the number of voxels within each bin, and plotted frequency as a function of bin number. We kept the range of rCBV values along abscissa constant (0–10) to calculate the following normalized histogram metrics: mode (rCBV with greatest frequency), maximum (greatest rCBV value), and histogram width (difference between maximum and minimum rCBV values).[18]

Statistical Analyses

Figure 2 provides a flow chart summarizing the major statistical analyses between the initial (training) set, the validation set, and the entire cohort. We calculated Pearson correlations between histologic tumor fraction and all pMRI-based metrics for all patients. We used the date of surgical re-resection to determine overall
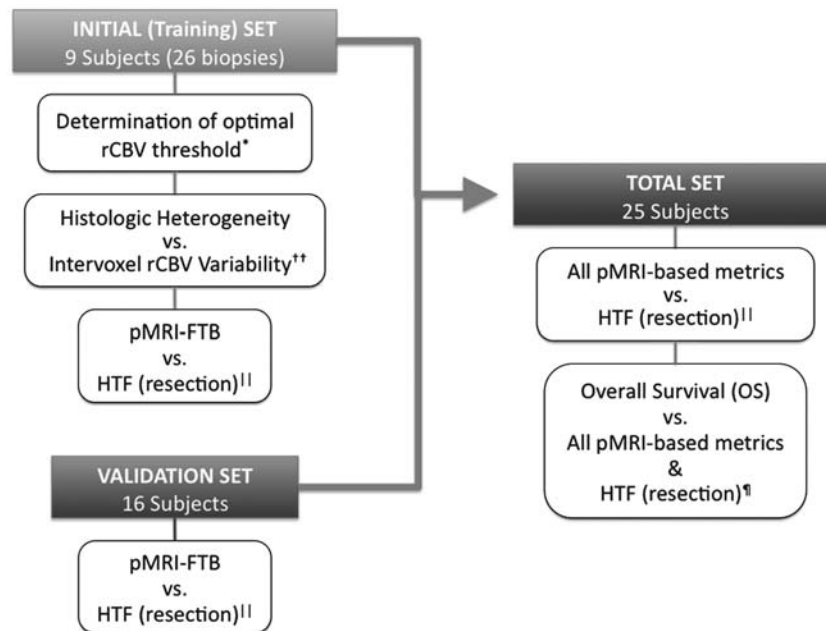

Fig. 2. Flow chart depicting the data collection and analyses for initial (training) and validation data sets, as well as the entire patient cohort. The initial (training) set was composed of 26 stereotactic biopsy samples from 9 subjects. Image coregistration enabled direct correlation between regions of interest (ROIs) on imaging and tissue analyses from corresponding biopsies. The validation data set was composed of 16 additional subjects but did not include stereotactic analysis. The total data set included patients from the initial and validation groups, and was composed of all 25 subjects. The (*) denotes the analysis that determined the most accurate rCBV threshold to distinguish biopsy specimens containing pure PTRE from those containing tumor. The (††) denotes that Pearson correlation was used to compare stereotactic biopsy results with coregistered, localized ROI analyses. The (∥) denotes that Pearson correlation was used to compare pMRI metrics from an entire CE-MRI enhancing lesion with histologic analyses from all submitted surgical resection tissue. The (¶) denotes that Cox-regression analyses were used to compare Overall Survival (OS) with all pMRI-based metrics from an entire CE-MRI enhancing lesion, as well as histologic analyses from all submitted surgical resection tissue.

survival (OS) and correlated OS with pMRI-based metrics using Cox regression. We assessed whether extent of surgical resection (i.e., total versus subtotal resection) was associated with OS via Cox regression analysis. We consider Cox regression to be the primary analysis method for determining correlations with outcome, because the metrics are treated as continuous variables without the use of predetermined categories or cutoff values. However, as a secondary method for determining correlations with outcome, we also used Log-rank tests to compare OS with histologic tumor fraction and all pMRI-based metrics. For each of these secondary analyses, we stratified patients into 2 categories (high or low) using the respective image-based or histologic-based group median values as cutoffs, with high categories having values above our patients' median and low categories having values equal to/less than the overall median. A biostatistician (AD) performed all analyses; statistical significance was indicated by $P < .05$.

RESULTS

Subject Population and Clinical Data

Twenty-five patients (18 males, 7 females) with recurrent GBM were recruited into the study, with a median age of 50 years (range, 25–73 years). Sixty-four percent of patients (16/25) developed progressively enlarging CE-MRI enhancing lesions within 6 months of initial TMZ-RT (range, 1.0–5.5 months; median, 4 months), whereas 36% (9/25) developed lesions more than 6 months post TMZ-RT (range, 8–53 months; median, 12 months). All patients underwent either total ($n = 11$) or subtotal ($n = 14$) resection of their posttherapy enhancing lesions. OS was not associated with extent of re-resection ($P = .79$), size of the enhancing CE-MRI lesion ($P = .56$), or patient age ($P = 0.26$). One of the 25 patients received prior bevacizumab for recurrent disease but failed this therapy, as evidenced by progressive increasing enhancement and mass effect on serial CE-MRI examinations prior to enrollment. We performed analyses both with and without inclusion of this patient; the pMRI correlations with histology and OS remained consistent under all conditions, thereby justifying this patient's inclusion. We report results for the complete cohort of 25 patients.

Optimal rCBV Threshold to Classify GBM and PTRE Voxels

Figure 3 shows that a threshold of 1.0 categorized stereotactic biopsy specimens as either tumor (>1.0) ($n = 17$) or PTRE (≤ 1.0) ($n = 9$) with 100% accuracy (sensitivity = 100%, 95%CI = 80.5–100%; specificity = 100%, 95%CI = 66.4–100%) based on the initial set of 26 stereotactic biopsies (from 9 subjects) and corresponding rCBV values. This threshold was used for all subsequent pMRI-FTB analyses to classify individual voxels as either tumor or PTRE.
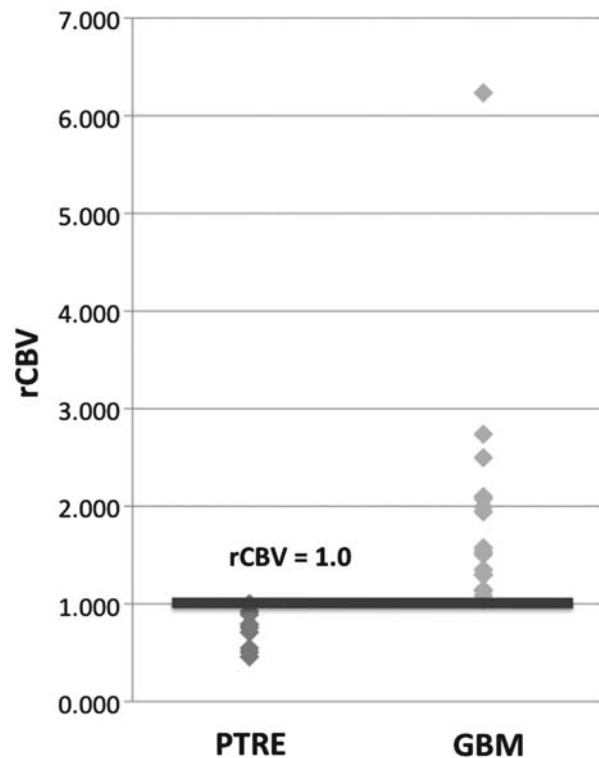

Fig. 3. Optimal rCBV Threshold to classify GBM and PTRE voxels: We established the relationship between rCBV and histopathologic diagnosis from an intial subset of 26 stereotactic biopsy samples through careful coregistration of pMRI ROIs and stereotactic locations, using nine-voxel-sized ROIs ($\sim$0.18 cm^3) to approximate tissue specimen volume ($\sim$0.2 cm^3). We averaged rCBV across nine voxels to minimize coregistration error while enabling separation of pure PTRE from tumor specimens with no rCBV overlap. The threshold of 1.0 separated specimens categorized as "tumor:" ($n = 17$) or "PTRE" ($n = 9$) with 100% accuracy (sensitivity = 100%, 95%CI = 80.5–100%; specificity = 100%, 95%CI = 66.4–100%). The PTRE values clustered tightly at and below the rCBV threshold of 1.0, suggesting there was histologic homogeneity across specimens. In contrast, rCBV in GBM varied broadly above 1.0 suggesting variability in tumoral angiogenesis and the degree of histologic admixture with PTRE.

Correlating Intervoxel rCBV Variability and Histologic Heterogeneity for Stereotactic Biopsy Samples Containing Tumor

The rationale for using stereotactic coregistration to compare localized pMRI measurements with the stereotactic biopsies was to minimize the risk of sampling error that might confound the correlation between imaging and tissue analysis. Of the initial 26 biopsy specimens (from 9 patients) described above, 9 biopsies contained pure PTRE and 17 biopsies contained some degree of tumor that varied in regards to histologic tumor fraction (median = 75%; range, 1%–100%). For all tumor biopsies, the mean rCBV value from each ROI was >1.0 threshold (group median = 1.5; range = 1.02–5.72), although in some ROIs, there was variability in the number of individual voxels that were >1.0.

Specifically, some tumor biopsy ROIs demonstrated a relatively higher percentage of voxels equal to or below threshold (i.e., PTRE voxels), compared with other samples with relatively more ROI voxels above threshold (i.e., tumor voxels). For each ROI, we found that the percentage of tumor voxels (median = 89%; range, 22%–100%) correlated with the histologic tumor fraction from corresponding biopsy specimens ($n = 17$, $r = 0.72$, $P < .002$).

To adjust for potential bias resulting from a different number of tissue samples collected from each subject, we performed a bootstrap analysis in which Pearson correlations were computed with random selection of one specimen per subject. For the comparison between percentage of tumor voxels and histologic tumor fraction within each biopsy, the correlation remained consistent with the original analysis (average $r = 0.68$, standard error = 0.003). This suggests that intrasubject grouping effects, if present, did not significantly bias the correlations across the entire group of specimens. The rCBV mean (of all 9 voxels) for each ROI correlated poorly with histologic tumor fraction ($n = 17$, $r = 0.36$, $P = .17$). Figure 4 shows an example of rCBV variability in corresponding biopsy samples with high and low histologic tumor fraction.

Correlations between pMRI-Based Metrics, Histologic Tumor Fraction, and OS

For all 25 patients, we quantified histologic tumor fraction from the combination of all submitted surgical resection material and stereotactic biopsies. Histologic tumor fraction most strongly correlated with pMRI-FTB ($r = 0.82$, $P < .0001$), compared with other pMRI-based metrics, as summarized in Table 1 and in Fig. 5. The initial (training) subset of 26 biopsy samples (from 9 subjects) was included in this analysis, because the biopsies represented only a fraction of submitted surgical tissue from the respective patients. Nonetheless, to test whether the correlation between histologic tumor fraction and pMRI-FTB significantly differed between the subjects in the initial training set ($n = 9$) versus those not in the training set ($n = 16$), we performed separate Pearson correlations for each of these 2 groups (summarized in the footnote of Table 1). Because these correlations for the 2 groups were essentially identical ($n = 9$, $r = 0.84$, $P < .01$ and $n = 16$, $r = 0.82$, $P < .001$, respectively), it was highly unlikely that the correlation in the training set was disproportionately driving that of the entire cohort.

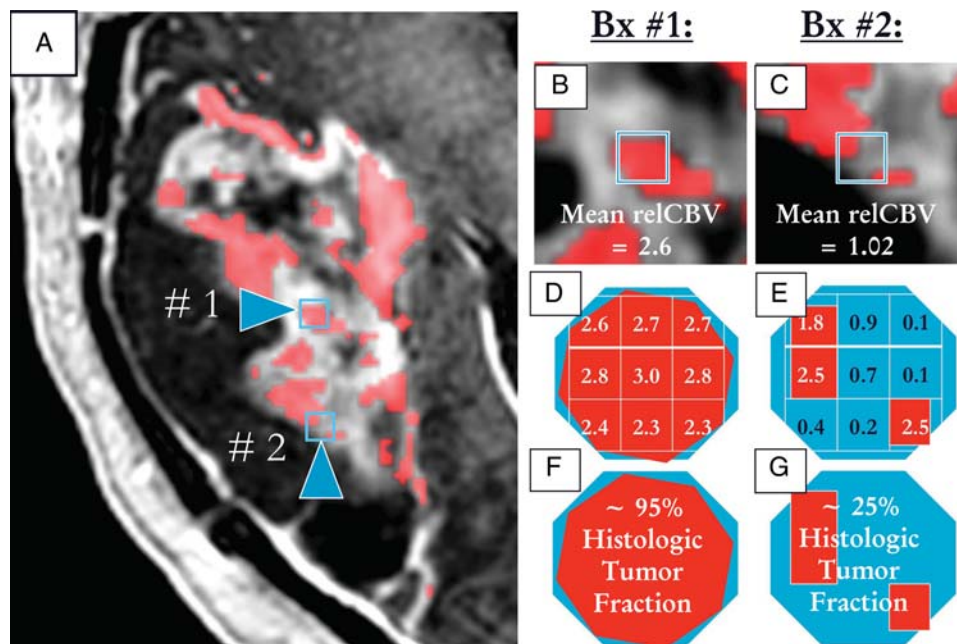Figure 6 shows an example of pMRI-FTB maps in 2 patients with different histologic tumor fractions from

Fig. 4. Two recurrent GBM stereotactic biopsies showing different histologic tumor fractions and rCBV measurements. (A) Coregistration of pMRI-FTB and neuronavigational images enabled demarcation of voxels predictive of tumor (red), based on rCBV values above the threshold of 1.0. (B,C) We measured rCBV at two biopsy locations (boxes with arrowheads) defined by nine-voxel Regions of Interest (ROIs). In magnified views of the ROIs mean rCBV for both biopsies were above 1.0, corresponding to the presence of tumor within each sample. (D,E) When analyzing individual voxels comprising each ROI, biopsy #2 (E) demonstrated greater intervoxel rCBV variability compared with biopsy #1 (D), such that the percentage of voxels above threshold (red) was lower for biopsy #2 (E). The lower percentage of tumor voxels on pMRI correlated with lower histologic tumor fraction within the biopsy sample (F,G). The data from Figs 3 and 4 suggest that rCBV thresholding can be applied, not only to multi-voxel ROIs, but also to single voxels to exclude the presence of tumor. In this study, single-voxel thresholding depicts histologic tumor fraction more accurately than the mean rCBV from nine-voxel ROIs, by identifying subregions of PTRE at nine-fold higher spatial resolution.

Table 1. Summary of correlations between pMRI-based metrics, histologic tumor fraction, and overall survival (OS)

Metric	Median value (range)	Correlation with Histologic Tumor Fraction (P value)	P value for correlation with OS*
Histologic Tumor Fraction	49% (0–98)	–	<0.03
pMRI-FTB	63% (16–99)	$r = 0.82$ ** $(P < .0001)$	<0.02
Mean rCBV	1.6 (0.6–4.7)	$r = 0.57 (P < .01)$	Ns (0.45)
Histogram Mode (rCBV)	1.1 (0.06–4.5)	$r = 0.62 (P < .001)$	Ns (0.17)
Histogram Width (rCBV)	9.9 (3.8–20.4)	$r = 0.08 (P = .69)$	Ns (0.28)
Histogram Max (rCBV)	9.9 (3.8–20.4)	$r = 0.08 (P = .69)$	Ns (0.28)

*Based on Cox-regression analysis.
*"Ns" denotes Nonsignificant survival correlation.
**The correlation listed in the table is for the entire cohort of 25 subjects. The correlation among subjects in the initial training set ($n = 9$) was $r = 0.84$, $P < 0.01$; the correlation among subjects not in the training set ($n = 16$) was $r = 0.82$, $P < .001$.
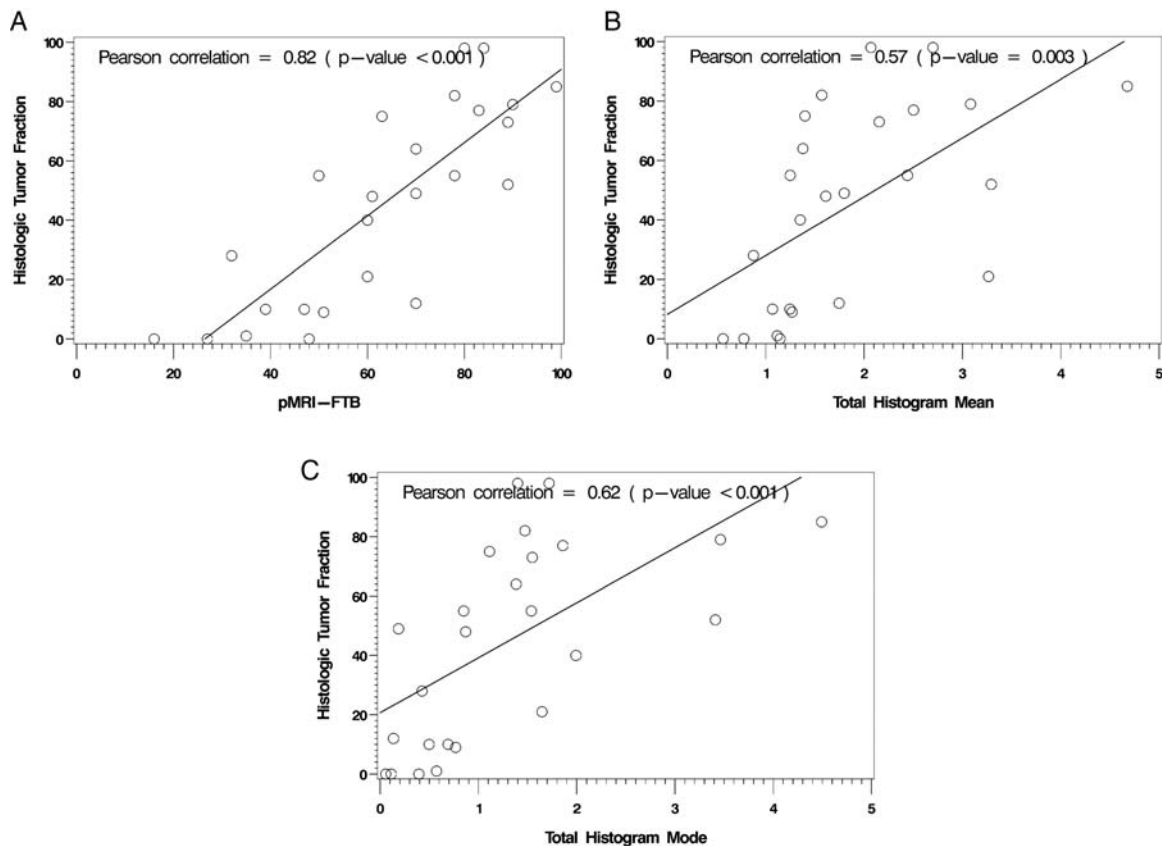

Fig. 5. Pearson correlations between histologic tumor fraction and different pMRI-based metrics. The scatterplot graphs demonstrate that histologic tumor fraction correlates most strongly with pMRI-FTB (A), compared with mean rCBV (B) and histogram mode rCBV (C). The r correlation coefficients and p values are included in the respective graphs.

surgical specimens. At the time of this analysis, 15 patients had died. Median clinical follow-up for living patients was 455 days from the time of initial treatment and 151 days from the time of surgical re-resection. OS was significantly associated with only histologic tumor fraction ($P < .03$) and pMRI-FTB ($P < .02$), but not with mean rCBV or any other histogram analysis metrics (Cox regression analysis). Qualitatively, the distributions of the rCBV histograms were generally unimodal and similar to previous reports.[18,19] Histogram width was nearly identical to

histogram maximum value, as minimum values for all histograms were close to zero. Table 1 summarizes the range and group median values for histologic tumor fraction, pMRI-based metrics, and their correlations with OS. Secondary analyses using Log-rank test demonstrated significantly shorter OS in patients with high pMRI-FTB (above the group median of 63%, $P < .03$) or high histologic tumor fraction (above the group median of 49%, $P < .04$), compared with counterparts with low values. Log-rank survival analyses were not significant for rCBV
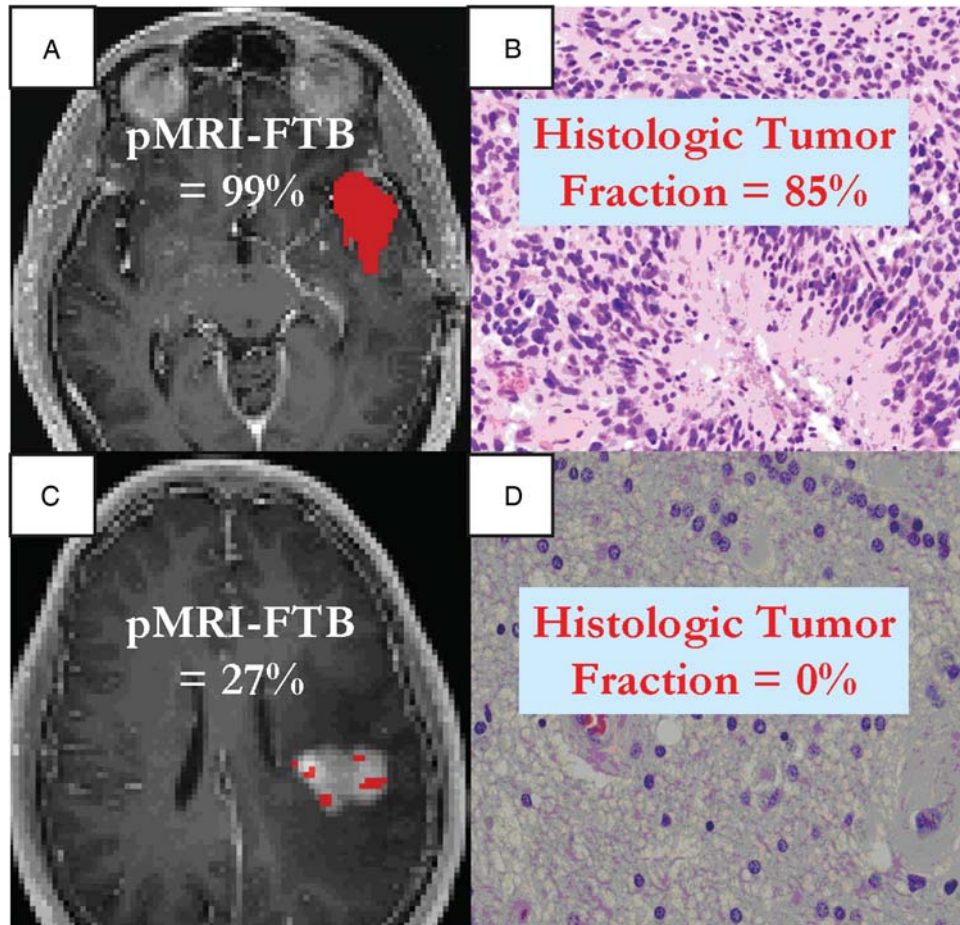
Fig. 6. Measures of pMRI-FTB and histologic tumor fraction from two patients with CE-MRI enhancing lesions suspicious for recurrent GBM. (A,C) Color pMRI-FTB maps depict red voxels as those with rCBV above threshold that are predictive of tumor. The pMRI-FTB metric represents the percentage of tumor voxels relative to total enhancing CE-MRI lesion voxels. In the first patient, pMRI-FTB of 99% (A) correlated with high histologic tumor fraction of 85% (B). In contrast, the second patient demonstrated low pMRI-FTB (C) and low histologic tumor fraction (D). These cases illustrate the utility of pMRI-FTB to noninvasively estimate tumor burden as a fractional subcomponent of otherwise nonspecific CE-MRI lesions.

mean ($P=.37$), mode ($P = .25$), maximum ($P = .28$), or histogram width ($P = .28$).

Discussion

This study correlated multiple, distinct pMRI-based metrics with histologic tumor fraction and OS in a cohort of patients with recurrent GBM undergoing surgical re-resection for suspected tumor regrowth. Unlike prior studies,[16,18,20,27,28] we did not use predetermined histologic tumor fraction categories, because we chose not to assume prior knowledge of which histologic criteria would be clinically relevant to OS. Instead, we directly compared the imaging and histologic measures as continuous variables to identify broad correlations with OS and any potential pMRI-based predictors of outcome for future validation studies. Overall, pMRI-FTB provided the most robust estimate of histologic tumor fraction and was the only imaging metric that correlated with OS. Other pMRI-based metrics,

such as rCBV mean and mode, correlated less strongly with histology and did not correlate with OS. Our findings that pMRI-FTB and histologic tumor fraction both correlate with OS suggest that both are good indicators of tumor progression and clinical prognosis. We intend to validate the correlation between pMRI-FTB and survival in future clinical trials.

There are few reports in the literature attempting to correlate pMRI methodologies with histologic tumor fraction and CE-MRI lesions in patients with recurrent GBM. Virtually all studies view CE-MRI lesions as either tumor or PTRE, although the vast majority of lesions are in fact histologically admixed and broadly variable in tumor fraction.[18,27–29] Thus, the literature proposes lesion categorization criteria that depend on various histologic tumor fraction cutoff values. In general, image-based studies have preserved these cutoff values, but have not considered survival relationships. This has resulted in variable histologic standards, making unbiased comparison of pMRI-based metrics difficult. For example, Barajas et al.[16] studied mean

rCBV and chose a 5% cutoff to classify CE-MRI lesions as tumor, whereas Gasperetto et al.[20] studied rCBV thresholding and chose a 20% cutoff. Kim et al.[18] studied various histogram-based metrics, but chose to separate CE-MRI lesions into three histologic categories, based on the histologic tumor fraction ranges of <20%, 20–50%, and >50%. Because these studies did not correlate results with survival, their underlying clinical justification may be limited.

Prior histology-based studies suggest that cutoff values guiding lesion classification can impact the relationship between tumor fraction and survival.[12–15] Tihan et al. evaluated a 25% cutoff in a cohort of patients with recurrent GBM and reported no survival difference between radionecrosis and tumor groups.[15] Forsyth et al. reported significant group survival differences using a 75% cutoff, although the cohort consisted of mixed tumor grades (II-IV).[12] Kim et al. recently reported survival differences within a cohort of 20 patients with recurrent GBM, using 3 histlologic categories based on the cutoff values of <20% and >80% recurrent tumor fraction.[14] Because these studies, to our knowledge, comprise the world literature correlating histologic tumor fraction with prognosis, further investigation is warranted, particularly in recurrent GBM cohorts. The Cox regression analysis from our pilot study suggests that histologic tumor fraction (like pMRI-FTB) correlates directly with survival, irrespective of classification methods and predetermined cutoff values. As further proof of concept, our secondary analyses using Log-rank tests suggest that the histologic cutoff of 50% was predictive of survival in our cohort; however, we are wary to recommend the prospective use of any particular cutoff value, until these data can be validated in a larger GBM population.

The relationships between rCBV, histologic tumor fraction, and clinical outcome warrant further discussion. In this study, we specifically evaluated the utility of rCBV (as analyzed by various methods) to estimate histologic tumor fraction as a predictor of outcome. Compared to the pMRI-FTB metric, the magnitude of mean rCBV showed weaker correlation with histologic tumor fraction. This is because mean rCBV (similar to other histogram-based metrics) is influenced by the magnitude of rCBV from both tumoral and nontumoral (PTRE) components. In addition, GBM exhibits microvascular heterogeneity and broad rCBV variability even among tumor subregions,[30–33] and the calculation of mean rCBV is susceptible to biases from extremely high or low values, even in a relatively small population of voxels. In contrast, rCBV magnitude has less impact on the calculation of pMRI-FTB, except to classify voxels according to minimum threshold requirements. This approach more purely approximates the volume of tumor burden by mitigating influences from varying degrees of tumoral angiogenesis. As an example, a voxel with rCBV of 1.2 will be classified as tumor in the same manner as another voxel with rCBV of 12.0.

We must also address the fact that tumoral angiogenesis and rCBV magnitude are well-established, independent prognostic markers in newly diagnosed and recurrent glioma.[33–35] In a previous study that used stereotactic analysis to correlate rCBV with tumor micro-vasculature, both rCBV magnitude and microvessel area predicted OS in a cohort of patients with recurrent high-grade glioma.[33] However, our current study did not show a correlation between rCBV magnitude (i.e., mean) and OS. A plausible explanation is that the previous study excluded regions of PTRE from rCBV and histologic analyses. Unlike our current study, their mean rCBV calculations did not include potentially confounding contributions from PTRE components, which may have helped to retain the prognostic value of rCBV magnitude within tumor. Further studies are likely warranted to distinguish histologic tumor fraction and degree of angiogenesis as separate and independent prognostic indicators in recurrent GBM. Besides measuring rCBV at a single time, other groups have also shown the prognostic value of assessing the magnitude of change in rCBV before and after treatment.[34,35]

In the current study, we used careful stereotactic coregistration to establish the rCBV threshold of 1.0 that differentiates PTRE and tumor specimens with 100% accuracy. The current rCBV threshold is slightly higher than the one that we previously reported.[21] In the current study, we optimized several postprocessing steps to increase the clinical robustness and reproducibility of pMRI analysis across institutions, and to help streamline clinical workflow. We also chose to normalize CBV only to normal appearing white matter (NAWM). This method differs from prior use of both gray matter (GM) and NAWM for normalization,[21] but has been shown to provide greater rCBV measurement stability under varied pMRI acquisition conditions.[24] Because GM has higher microvascular volume, compared with NAWM, the rCBV values will be inherently lower when normalizing against GM, as opposed to NAWM.[24] In addition, we used a commercially available software package that corrected T2/T2*W residual effects with a modeling algorithm, compared with prior use of baseline-subtraction (BLS). Modeling correction, compared with BLS, does not require manual user input to define the first pass interval of the contrast bolus, thereby reducing operator-dependent variability and overall postprocessing time.[21,23,24] It is also possible that these methodological differences may have contributed to the differences in rCBV threshold.[22–24] Of note, although the thresholds varied slightly between studies, the accuracy to distinguish GBM from PTRE remained consistently high. We feel that the current methods described here, using the rCBV threshold of 1.0, enable robust calculation of pMRI-FTB on a clinical basis and across multiple institutions.

Since the adoption of combined TMZ and RT as standard adjuvant treatment for GBM, there has been increasing awareness of therapy-related parenchymal injury, so called PTRE, which mimics tumor regrowth on CE-MRI. PTRE results from treatment-induced tumor and endothelial-cell death that causes vasogenic edema and enhancement on CE-MRI.[7–10] Both pP and RN are widely described forms of PTRE that mimic tumor regrowth but differ in timing and severity. The

mild and self-limited pP develops within 3–6 months of RT, often before adjuvant TMZ is completed. Thus, erroneous interpretation of pP as treatment failure can lead to premature cessation of chemotherapy.[8,9,13] In contrast, RN develops >6 months after RT and is more severe, typically requiring steroids or surgical debulking. The development of pP markedly increases the risk for subsequent RN, supporting shared pathophysiology between the 2 entities.[8,9,13] In our cohort, the vast majority of lesions contained histologic admixture between tumor and PTRE, with most lesions developing during the time frame of pP.

The reliance on conventional imaging to distinguish tumor from PTRE leads to diagnostic inaccuracy and potential clinical inefficiency. For instance, the proposed workaround to the poor accuracy of CE-MRI is to use serial changes in lesion size over multiple CE-MRI examinations to distinguish pP from tumor, based on the premise that lesions decreasing in size likely represent pP;[6–9] however, histologic admixture in the vast majority of lesions often degrades the accuracy of this approach. Specifically, the pP subcomponents within an admixed lesion may decrease in size over time, whereas the tumoral subcomponents may increase. In addition, it is not uncommon for PTRE or indolent tumor to remain stable over time. Thus, the overall size of a CE-MRI lesion is the sum of dynamic changes from multiple competing histologic processes that makes it difficult to accurately judge tumor burden. In addition, serial imaging requires months to reach a diagnosis, during which time tumor progression may have occurred. Consequent delay in appropriate therapy may ultimately reduce treatment efficacy or increase toxicity, because the tumor invades surrounding brain parenchyma. Compared with serial CE-MRI examinations, pMRI-FTB can estimate tumor burden in an accurate and timely manner during a single examination. This may provide a useful imaging endpoint for defining PFS and predicting OS in future clinical trials.[1–3]

We recognize several potential limitations to this study. Despite high correlation between pMRI-FTB and histologic tumor fraction, pMRI-FTB was consistently higher than the histologic tumor fraction. This might be explained by resolution differences between pMRI (millimeters) and histology (microns). In addition, it is possible that sampling errors resulted in consistent underestimation of tumor burden on histology; these errors would not affect pMRI-FTB, which can assess CE-MRI lesions

in their entirety. The patient sample size was small, and these results should be validated in a larger GBM population. There could have been small misregistration errors between localized pMRI ROI placement and the stereotactic biopsy locations, caused by errors in coregistration, image distortions and brain shift following craniotomy. To compensate, neurosurgeons used small craniotomy sizes to minimize brain shift and also visually validated stereotactic image location with intracranial neuroanatomical landmarks to help correct for random brain shifts. Rigid-body coregistration of stereotactic and DSC-MRI also helped reduce possible geometric distortions. Thus, the misregistration in this study was likely no greater than 1–2 mm and similar to that of previous studies using stereotactic biopsy.[21,27,28,32]

Conclusion

pMRI-FTB can reliably estimate histologic tumor fraction within otherwise nonspecific CE-MRI enhancing lesions. Our study shows that quantifying tumor burden, relative to components of pseudoprogression and radiation necrosis, can help to predict survival in the setting of recurrent GBM. This suggests that pMRI-FTB represents a promising noninvasive biomarker of tumor progression and clinical outcome, which could prove to be useful in future clinical trials and in the management of recurrent GBM.

References

1. Lang FF, Gilbert MR, Puduvalli VK, et al. Toward better early-phase brain tumor clinical trials: a reappraisal of current methods and proposals for future strategies. *Neuro Oncol*. 2002;4(4):268–277.

2. Polley MY, Lamborn KR, Chang SM, et al. Six-month progression-free survival as an alternative primary efficacy endpoint to overall survival in newly diagnosed glioblastoma patients receiving temozolomide. *Neuro Oncol*. 2010;12(3):274–282.

3. Ballman KV, Buckner JC, Brown PD, et al. The relationship between six-month progression-free survival and 12-month overall survival end points for phase II trials in patients with glioblastoma multiforme. *Neuro Oncol*. 2007;9(1):29–38.

4. Stupp R, Mason WP, van den Bent MJ, et al. Radiotherapy plus concomitant and adjuvant temozolomide for glioblastoma. *N Engl J Med*. 2005;352(10):987–996.

5. Macdonald DR, Cascino TL, Schold SC, Jr, Cairncross JG. Response criteria for phase II studies of supratentorial malignant glioma. *J Clin Oncol*. 1990;8(7):1277–1280.

6. Wen PY, Macdonald DR, Reardon DA, et al. Updated response assessment criteria for high-grade gliomas: response assessment in neuro-oncology working group. *J Clin Oncol*. 2010;28(11):1963–1972.

7. Clarke JL, Chang S. Pseudoprogression and pseudoresponse: challenges in brain tumor imaging. *Curr Neurol Neurosci Rep*. 2009;9(3):241–246. Review.

8. Brandsma D, van den Bent MJ. Pseudoprogression and pseudoresponse in the treatment of gliomas. *Curr Opin Neurol*. 2009;22(6): 633–638.

9. Brandsma D, Stalpers L, Taal W, et al. Clinical features, mechanisms, and management of pseudoprogression in malignant gliomas. *Lancet Oncol*. 2008;9(5):453–461.

10. Brandes AA, Franceschi E, Tosoni A, et al. MGMT promoter methylation status can predict the incidence and outcome of pseudoprogression after concomitant radiochemotherapy in newly diagnosed glioblastoma patients. *J Clin Oncol*. 2008;26(13):2192–2197.

11. Burger PC, Mahley MS, Jr, Dudka L, Vogel FS. The morphologic effects of radiation administered therapeutically for intracranial gliomas: a postmortem study of 25 cases. *Cancer*. 1979;44(4): 1256–1272.

12. Forsyth PA, Kelly PJ, Cascino TL, et al. Radiation necrosis or glioma recurrence: is computer-assisted stereotactic biopsy useful? *J Neurosurg*. 1995;82(3):436–444.

13. Perry A, Schmidt RE. Cancer therapy-associated CNS neuropathology: an update and review of the literature. *Acta Neuropathol*. 2006; 111(3):197–212.

14. Kim JH, Kim YB, Han JH, et al. Pathologic Diagnosis of Recurrent Glioblastoma: Morphologic, Immunohistochemical, and Molecular Analysis of 20 Paired Cases. *Am J Surg Pathol*. 2012;36(4):620–628.

15. Tihan T, Barletta J, Parney I, et al. Prognostic value of detecting recurrent glioblastoma multiforme in surgical specimens from patients after radiotherapy: should pathology evaluation alter treatment decisions? *Hum Pathol*. 2006;37(3):272–282.

16. Barajas RF, Jr, Chang JS, Segal MR, et al. Differentiation of recurrent glioblastoma multiforme from radiation necrosis after external beam radiation therapy with dynamic susceptibility-weighted contrast-enhanced perfusion MR imaging. *Radiology*. 2009;253(2): 486–496.

17. Sugahara T, Korogi Y, Tomiguchi S, et al. Posttherapeutic intraaxial brain tumor: the value of perfusion-sensitive contrast-enhanced MR imaging for differentiating tumor recurrence from nonneoplastic contrast-enhancing tissue. *AJNR Am J Neuroradiol*. 2000;21(5):901–909.

18. Kim HS, Kim JH, Kim SH, et al. Posttreatment high-grade glioma: usefulness of peak height position with semiquantitative MR perfusion histogram analysis in an entire contrast-enhanced lesion for predicting volume fraction of recurrence. *Radiology*. 2010; 256(3):906–915.

19. Emblem KE, Nedregaard B, Nome T, et al. Glioma grading by using histogram analysis of blood volume heterogeneity from MR-derived cerebral blood volume maps. *Radiology*. 2008;247(3):808–817.

20. Gasparetto EL, Pawlak MA, Patel SH, et al. Posttreatment recurrence of malignant brain neoplasm: accuracy of relative cerebral blood volume fraction in discriminating low from high malignant histologic volume fraction. *Radiology*. 2009;250(3):887–896.

21. Hu LS, Baxter LC, Smith KA, et al. Relative cerebral blood volume values to differentiate high-grade glioma recurrence from posttreatment radiation effect: direct correlation between image-guided tissue histopathology and localized dynamic susceptibility-weighted contrast-enhanced perfusion MR imaging measurements.. *AJNR Am J Neuroradiol*. 2009;30(3):552–558.

22. Boxerman JL, Schmainda KM, Weisskoff RM. Relative cerebral blood volume maps corrected for contrast agent extravasation significantly correlate with glioma tumor grade, whereas uncorrected maps do not. *AJNR Am J Neuroradiol*. 2006;27(4):859–867.

23. Paulson ES, Schmainda KM. Comparison of dynamic susceptibility-weighted contrast-enhanced MR methods: recommendations for measuring relative cerebral blood volume in brain tumors. *Radiology*. 2008;249(2):601–613.

24. Hu LS, Baxter LC, Pinnaduwage DS, et al. Optimized preload leakage-correction methods to improve the diagnostic accuracy of dynamic susceptibility-weighted contrast-enhanced perfusion MR imaging in posttreatment gliomas. *AJNR Am J Neuroradiol*. 2010;31(1):40–48.

25. Kassner A, Annesley DJ, Zhu XP, et al. Abnormalities of the contrast recirculation phase in cerebral tumors demonstrated using dynamic susceptibility contrast-enhanced imaging: a possible marker of vascular tortuosity. *J Magn Reson Imaging*. 2000;11(2):103–113.

26. World Health Organization. ICD-O:WHO Classification of Tumors, 4th ed. Geneva, Switzerland: World Health; 2006.

27. Rock JP, Hearshen D, Scarpace L, et al. Correlations between magnetic resonance spectroscopy and image-guided histopathology, with special attention to radiation necrosis. *Neurosurgery*. 2002;51(4):912–919; discussion 919–20.

28. Rock JP, Scarpace L, Hearshen D, et al. Associations among magnetic resonance spectroscopy, apparent diffusion coefficients, and image-guided histopathology with special attention to radiation necrosis. *Neurosurgery*. 2004;54(5):1111–1117; discussion 1117–9.

29. McGirt MJ, Bulsara KR, Cummings TJ, et al. Prognostic value of magnetic resonance imaging-guided stereotactic biopsy in the evaluation of recurrent malignant astrocytoma compared with a lesion due to radiation effect. *J Neurosurg*. 2003;98(1):14–20.

30. Lupo JM, Cha S, Chang SM, Nelson SJ. Dynamic susceptibility-weighted perfusion imaging of high-grade gliomas: characterization of spatial heterogeneity. *AJNR Am J Neuroradiol*. 2005;26(6):1446–1454.

31. Wesseling P, van der Laak JA, de Leeuw H, et al. Quantitative immunohistological analysis of the microvasculature in untreated human glioblastoma multiforme. Computer-assisted image analysis of whole-tumor sections. *J Neurosurg*. 1994;81(6):902–909.

32. Sadeghi N, Salmon I, Decaestecker C, et al. Stereotactic comparison among cerebral blood volume, methionine uptake, and histopathology in brain glioma. *AJNR Am J Neuroradiol*. 2007;28(3):455–461.

33. Hu LS, Eschbacher JM, Dueck AC, et al. Correlations between perfusion MR imaging cerebral blood volume, microvessel quantification, and clinical outcome using stereotactic analysis in recurrent high-grade glioma. *AJNR Am J Neuroradiol*. 2012;33(1):69–76.

34. Mangla R, Singh G, Ziegelitz D, et al. Changes in relative cerebral blood volume 1 month after radiation-temozolomide therapy can help predict overall survival in patients with glioblastoma. *Radiology*. 2010;256(2): 575–584.

35. Galbán CJ, Chenevert TL, Meyer CR, et al. Prospective analysis of parametric response map-derived MRI biomarkers: identification of early and distinct glioma response patterns not predicted by standard radiographic assessment. *Clin Cancer Res*. 2011;17(14):4751–4760.